Pressure-stabilized unconventional stoichiometric yttrium sulfides

Ju Chen,[1] Wenwen Cui,[1,*] Kun Gao,[1] Jian Hao,[1] Jingming Shi,[1] and Yinwei Li[1,2,†]

[1]*Laboratory of Quantum Functional Materials Design and Application, School of Physics and Electronic Engineering, Jiangsu Normal University, Xuzhou 221116, China*

[2]*Shandong Key Laboratory of Optical Communication Science and Technology, School of Physical Science and Information Technology of Liaocheng University, Liaocheng 252059, China*

(Received 12 October 2020; revised 1 December 2020; accepted 14 December 2020; published 29 December 2020)

Yttrium sulfides are found to exhibit rich phase diagram and diverse properties under pressures. Here, we systematically investigate the stability of binary Y-S system up to 50 GPa using first-principles swarm-intelligence structure search. We identify seven hitherto unknown stoichiometries (Y_7S_6, Y_6S_5, Y_7S_8, Y_6S_7, Y_5S_6, Y_3S_2, and YS_3) that are energetically stable with respect to the decomposition into elemental components. All phases exhibit metallic nature, of which YS_3 shows potential superconductivity with estimated T_c of 18.5 K at 50 GPa. The T_c in YS_3 is comparable to the 17 K superconductivity in elements yttrium (89.3 GPa) and sulfur (160 GPa), but could be achieved at much lower pressure. The high superconductivity is attributed to the high electronic density of states from S atoms at Fermi level. Additionally, Y_3S_2 is predicted to be a layer-structured magnetic electride with magnetic moment of 0.5 μB per formula unit at 6 GPa, which transforms to a three-dimensional phase with weak superconductivity around 17 GPa.

DOI: 10.1103/PhysRevResearch.2.043435

I. INTRODUCTION

Many efforts have been devoted to investigating high-T_c superconductors at extreme conditions, where high pressure is a powerful tool to stabilize the compounds that are inaccessible at ambient pressure. Recently, several theory-initiated discoveries of high-T_c hydrides superconductors, such as 203 K in H_3S at 150 GPa [1–3], 260 K in LaH_{10} at 170 GPa [4–7], and 224 K in YH_6 at 120 GPa [8–11], have brought about a new era of superconductors. However, because the superconductivities of these hydrides are only retained at extremely high pressure (>100 GPa), practical applications are a big challenge. Therefore, it is highly desirable to reduce the pressure at which superconductivity emerges.

Elements yttrium (Y) and sulfur (S) can transform to superconductors with same T_c of 17 K at 89.3 GPa and 160 GPa [12–14], respectively. The research on their binary yttrium sulfides is particularly fascinating, with four known phases (YS, Y_3S_4, Y_2S_3, and YS_2) available at ambient or high pressure [15–17]. As yttrium and sulfur have +3 and −2 oxidation states, respectively, the conventional stoichiometric Y_2S_3 is a semiconductor at ambient pressure. Studies show that the increased Y atomic fraction can significantly regulate the electronic properties, and all Y-S compounds with higher Y ratio as compared to Y_2S_3 show metallic nature. In particular, experiments show that the NaCl-type YS is a superconductor with T_c of 2 K at ambient pressure, which vanishes when transforming to the CsCl-type structure at 50 GPa [18–20]. Additionally, weak superconductivity (3.6 K) is also observed in the Th_3P_4-type Y_3S_4 that was synthesized at high pressure and high temperature [21]. However, YS_2 with higher S atomic fraction retains the semiconducting character.

Pressure is an effective tool to stabilize compounds with unconventional stoichiometries that possess exotic properties [22–26]. Here, we extensively investigate the crystal structures of various stoichiometric Y_xS_y ($x, y = 1$–8) at 0 and 50 GPa. In addition to the known compounds, the predictions uncover seven new thermodynamically stable compounds with stoichiometries Y_7S_6, Y_6S_5, Y_7S_8, Y_6S_7, Y_5S_6, Y_3S_2, and YS_3. Interestingly, an S-rich YS_3 is predicted to be a superconductor with T_c of 18 K at 50 GPa, close to that of elements Y and S, but could be achieved at much lower pressure. Additionally, the layer-structured Y-rich Y_3S_2 is found to be an electride with magnetism. The layer structure of Y_3S_2 transforms to a three-dimensional structure at 17 GPa, which shows weak superconductivity of 3 K at 20 GPa.

II. COMPUTATIONAL DETAILS

The crystal structure searches on Y_xS_y ($x, y = 1$–8) were performed by using crystal structure analysis by particle swarm optimization (CALYPSO) methodology [27–29], whose validity has been verified by correctly predicting predicting various crystal structures under high pressure [30–34]. In structure prediction runs, each generation contains 50 structures. For the first generation, the crystal structures are generated randomly with some symmetry constraints and

*wenwencui@jsnu.edu.cn
†yinwei_li@jsnu.edu.cn

subsequent optimizations. Then in the following generations, 60% of the structures with the lowest enthalpy through the particle swarm optimization algorithms are selected from the previous generation plus the 40% that are generated randomly to form the next generation. The structure search can be stopped when ≈1000 structures were generated and there are no new structures with lower energy. Structure relaxations and electronic structure calculations were performed using density functional theory within the Perdew-Burke-Ernzerhof (PBE) functional [35] in the framework of the all-electron projector augmented wave (PAW) method [36] as implemented in the VASP code [37]. The Y $4s^2 4p^6 5s^2 4d^1$ and S $3s^2 3p^4$ electrons were treated explicitly in all of the calculations. The plane-wave basis set with energy cutoffs of 700 and 1000 eV were employed for structure prediction and precise optimization, respectively. The k-point grids with density of 0.20 $Å^{-1}$ were generated using the the Monkhorst-Pack scheme [38]. The k meshes and energy cutoffs have been chosen to ensure that all the enthalpy calculations are well converged to 1 meV/atom. The electron-phonon coupling calculations were performed within the framework of the linear response theory through QUANTUM ESPRESSO code [39]. Ultrasoft pseudopotentials for Y and S were used with a kinetic cutoff energy of 100 Ry. The critical superconducting temperature, T_c, has been estimated using the Allen-Dynes modified McMillan equation [40]. The crystal structures and electron localization function (ELF) were plotted using VESTA software [41].

III. RESULTS AND DISCUSSION

An extensive variable-composition crystal structure search for Y_xS_y (x, y=1–8) was performed at 0 and 50 GPa. The maximum number of atoms in the simulation cell for each composition is no more than 24 atoms. The formation enthalpies of all considered Y-S compositions were calculated to construct the convex hulls, where a point lying on the tie line corresponds to a thermodynamically stable phase [Figs. 1(a) and 1(b)]. For those stoichiometries close to the convex hull, a fixed-composition structure search with a maximum four formula units (f.u.) per simulation cell was carried out to obtain the most stable structures. For those stable Y-S compounds deduced from the convex hulls, the relative enthalpies with respect to two neighboring stable compounds or elements were then calculated as functions of pressure in range of 0–60 GPa to obtain the phase diagrams as shown in Fig. 1(c). As expected, the known four compounds lie on the convex hull at ambient pressure, three (YS, Y_3S_4, and YS_2) of which stay thermodynamically stable up to 50 GPa [Fig. 1(b)]. However, the conventional stoichiometry Y_2S_3 possessing the lowest formation enthalpy at ambient pressure decomposes into Y_3S_4 and YS_2 at 8 GPa [Fig. 1(c)]. In addition to the known stoichiometries, the structure searches at ambient pressure identify five new thermodynamically stable compounds with stoichiometries Y_6S_5, Y_7S_6, Y_7S_8, Y_6S_7, and Y_5S_6. Among them, Y_6S_5 and Y_7S_6 are constructed by edge-sharing SY_6 octahedrons, while the other three by edge-sharing YS_6 octahedrons (please see the Supplemental Material, Fig. S1 [46]). Additionally, all five compounds are metallic with electronic density of states at Fermi level dominated by Y atoms

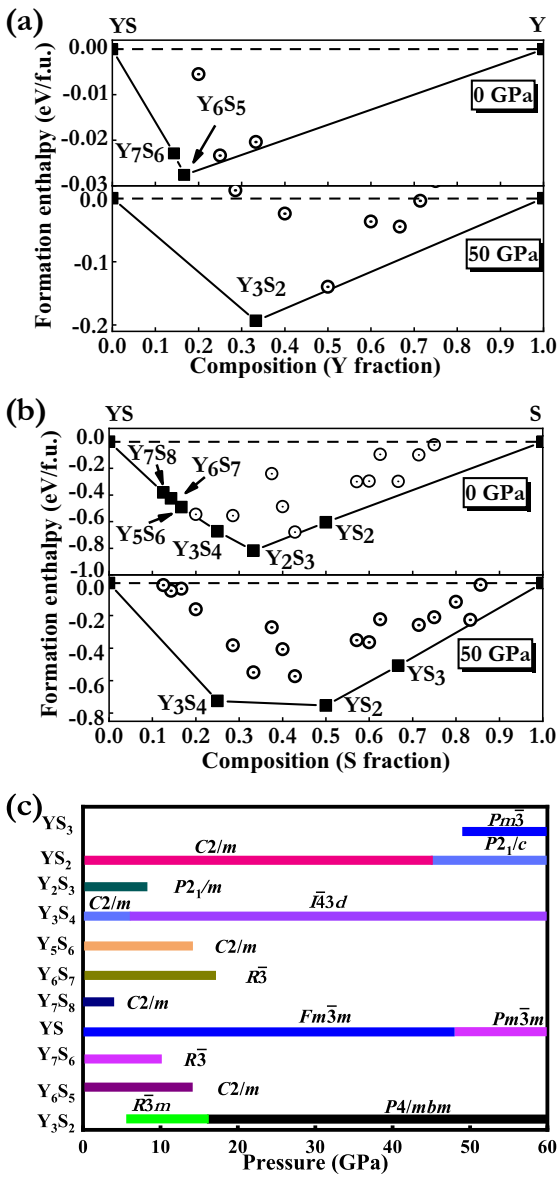

FIG. 1. The calculated formation enthalpies of various Y-S compounds with respect to YS + Y (a) and YS + S (b) at 0 and 50 GPa. The referenced structures of Y and S are taken from Refs. [18,21,42–45]. Panel (c) shows the phase diagrams of all phases as functions of pressure.

(Fig. S2). Phonon calculations confirm that all of them are dynamically stable without any negative frequencies (Fig. S3).

Structure searches at 50 GPa predict two new compounds, a Y-rich Y_3S_2 and an S-rich YS_3. Calculations show that Y_3S_2 become energetically stable at pressure as low as 6 GPa. The low-pressure phase of Y_3S_2 adopts hexagonal $R\bar{3}m$ structure, which is a layered structure consisting of edge-sharing SY_6 octahedrons [Fig. 2(a)]. Interestingly, the Y framework in Y_3S_2 is isostructural to high-pressure Sm-type Y phase [43,44]. Under compression, the layered $R\bar{3}m$ is overtaken by a three-dimensional tetragonal $P4/mbm$ structure at 17 GPa [Figs. 1(c) and 2(c)]. The coordination number of S increases from 6 in the $R\bar{3}m$ structure to 8 in the $P4/mbm$ structure, resulting in the formation of face-sharing SY_8 polyhedrons

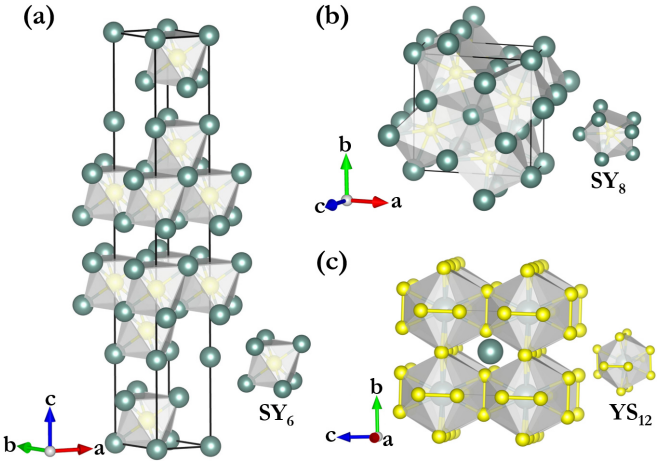

FIG. 2. The schematics of the $R\bar{3}m$ structure (a) and the $P4/mbm$ structure (b) of Y_3S_2, and the $Pm\bar{3}$ structure of YS_3 (c). Polyhedrons beside the structures represent the building blocks. The big gray-green and small yellow spheres represent Y and S atoms, respectively.

[Fig. 2(b)]. YS_3 possessing the cubic $Pm\bar{3}$ structure becomes energetically stable at 48 GPa [Fig. 1(c)]. Unlike other Y-S compounds, S_2 dimers are formed in YS_3 with S-S bond distance of 2.19 Å (50 GPa), close to that (≈2.17 Å) of S_8 ring-shaped molecules in phase I at 0 GPa [47]. Electron localization function (ELF) calculation reveals the covalent bond nature of S_2 dimer in view of the electron localization between two S atoms. The $Pm\bar{3}$ structure contains two inequivalent Y atoms that locate at the sites of a bcc lattice. Each Y atom occupying the bcc vertexes is surrounded by six S_2 dimers, forming a YS_{12} icosahedron with Y-S bond distance of 2.62 Å at 50 GPa. Another Y atom locates in the center of eight YS_{12} icosahedrons with a Y-S bond distance of 2.70 Å. Hereafter, the discussions will be focused on the two pressure-stabilized compounds, Y_3S_2 and YS_3, both of which are shown to possess exotic properties.

Both Y_3S_2 and YS_3 exhibit metallic features with bands crossing the Fermi level [Figs. 3(a)–3(c)]. For Y_3S_2, the DOS around the Fermi level in both the $R\bar{3}m$ and $P4/mbm$ structures are dominated by electrons from Y atoms, while the contribution from the S atoms is negligible. Interestingly, the layered $R\bar{3}m$-Y_3S_2 is a ferromagnetic metal in view of the different band structures and projected DOS of spin-up and spin-down electrons. The total magnetic moment of Y_3S_2 is calculated to be ≈0.5 μB per formula unit at 6 GPa and stays unchanged up to 17 GPa, the maximum stable pressure, which is mainly from the Y 4d orbitals. Interestingly, ELF results show that Y_3S_2 is an electride with dumbbell-like electrons localizing in the interstices of two neighboring SY_6 layers [Fig. 3(d)]. This kind of layer-structured magnetic electride is also found in Y_2C [45]. At the transformation to the $P4/mbm$ structure, the ferromagnetism of Y_3S_2 disappears deduced from the same profiles of spin-up and spin-down DOSs [Fig. 3(b)]. Simultaneously, no electron localizations are found in the interstices [Fig. 3(e)]. Different from that in Y_3S_2, the contribution to the Fermi level in YS_3 is mainly from S atoms, which is double that of Y atoms [Fig. 3(c)].

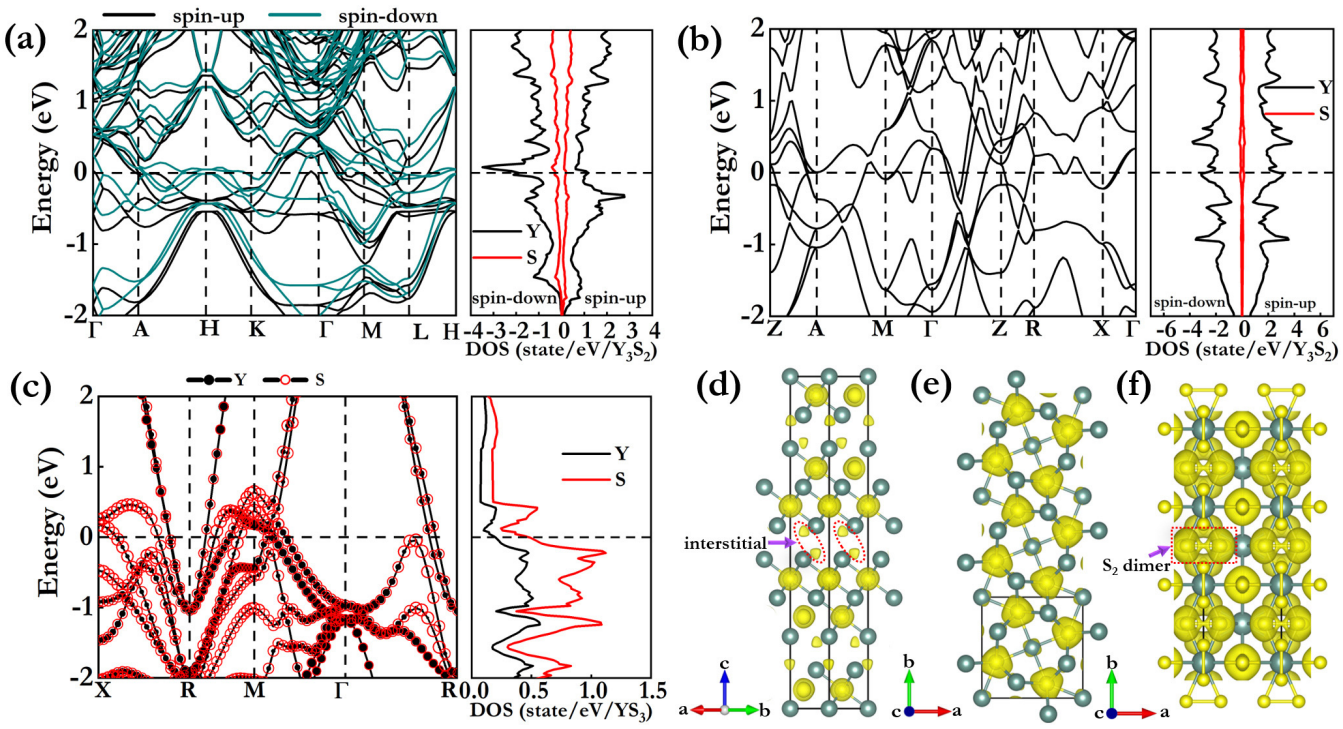

FIG. 3. The band structures and projected density of states (DOS) of the $R\bar{3}m$ structure of Y_3S_2 at 6 GPa (a), the $P4/mbm$ structure of Y_3S_2 at 50 GPa (b), and the $Pm\bar{3}$ structure of YS_3 at 50 GPa (c). Bands in panel (a) are divided into spin up and spin down, and the bands in panel (c) are projected onto Y and S atoms with circle radii proportional to the weights of the corresponding atoms. [(d)–(f)]Three-dimensional ELF of the three structures with isosurface value of 0.7.

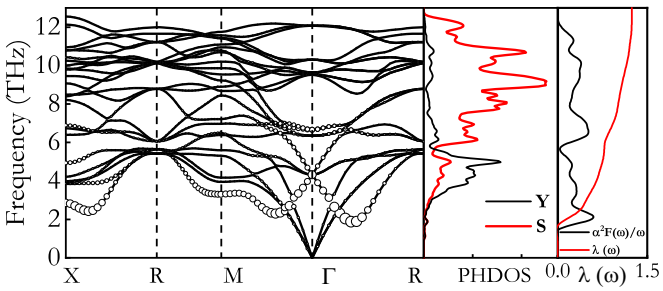

FIG. 4. The calculated phonon dispersion, projected phonon densities of states (PHDOS), Eliashberg spectral function $[\alpha^2F(\omega)/(\omega)]$, and EPC integration of $\lambda(\omega)$ for the $Pm\bar{3}$ structure of YS_3 at 50 GPa. Circles in the left panel indicate the phonon line width with radii proportional to the strength.

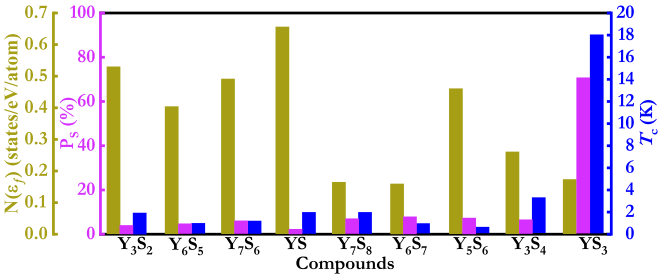

FIG. 5. The calculated T_c, the total DOS $N(\varepsilon_f)$ and the contribution of S atoms to the total DOS (P_S) at the Fermi level for the stable Y-S compounds. P_S is defined as the partial DOS of S atoms divided by the total DOS at the Fermi level.

Bader analysis shows that each Y atom donates averagely 1.74 electrons to S atoms in YS_3, much more than that (1.17) in Y_3S_2 (Table S1). The large charge transfer from Y atoms to S atoms explains the primary contribution of S atom to the Fermi level in YS_3.

The electron-phonon couplings (EPC) of $P4/mbm$-Y_3S_2 and $Pm\bar{3}$-YS_3 were calculated to examine their potential superconductivity, while that of the $R\bar{3}m$-Y_3S_2 was eliminated because of its magnetism. The electron-phonon coupling parameters λ of $P4/mbm$-Y_3S_2 is calculated to be 0.48 at 50 GPa, the same as that of the known superconductor Y_3S_4 (Table S2). The T_c value was then estimated using the Allen-Dynes modified McMillan equation [40] using a typical Coulomb pseudopotential of $\mu^* = 0.1$. Accordingly, the estimated T_c of $P4/mbm$-Y_3S_2 is ≈2.9 K, close to that (3.6 K [21]) of Y_3S_4.

Strikingly, we find that $Pm\bar{3}$-YS_3 has a relatively larger λ of 1.24 at 50 GPa, which leads to much higher T_c of 18.5 K as compared to Y_3S_2. Phonon dispersions and PHDOS show that the frequencies of $Pm\bar{3}$-YS_3 can be divided into two parts, with the low frequencies (<6 THz) dominated by vibrations of Y atoms, while the high end by vibrations of S atoms (Fig. 4). It is noteworthy that the low-frequency part contributes 64% to the total λ and mainly originates from the contribution of three Kohn anomalies that locate at X-R, M-Γ, and Γ-R high-symmetry directions. Considering the dominant DOS of S atoms at the Fermi level, we therefore conclude that the high superconductivity of YS_3 mainly originates from the coupling between the electrons of S atoms and phonon vibrations of Y atoms. The T_c estimated for YS_3 is comparable to the maximum 17 K for element Y (at 89.3 GPa) and S (at 160 GPa) but could be achieved at much lower pressure, indicating that alloying with other elements has the potential of decreasing the superconducting pressure. We have compared the volumes of YS_3 with those of elemental Y plus S at different pressures and found the incorporation of Y atoms has precompression effects on the S sublattice. For example, the volume of YS_3 at 50 GPa is calculated to be 53.80 Å^3, which is much smaller than that (61.74 Å^3) of Y plus S at the same pressure but is comparable to that (53.92 Å^3) at 160 GPa. In fact, this phenomenon is common in hydride superconductors, where the metallization can be achieved at lower pressure than with pure hydrogen, since the hydrogen atoms have already undergone chemical precompression by the heavy atoms [25,34,48]. Moreover, it is not unreasonable to deduce that hydrides of Y-S compounds have the potential to show high-T_c superconductivity at lower pressures.

The superconductivities of other stable Y-S compounds were also examined and the estimated T_c are summarized in Fig. 5. Unfortunately, all of them possess much lower superconductivities with T_c less than 4 K. Figure 5 also presents the total DOS as well as the contribution of S atoms to the total DOS at the Fermi level for all considered Y-S compounds. As compared to YS_3, all other Y-S compounds have comparable or even larger total DOS at the Fermi level. However, the contributions of S atoms to the total DOS in these compounds are negligible, completely distinct from the 75% contribution of S atoms in YS_3. The antipodal contribution of S atoms to the total DOS may explain the relatively high superconductivity in YS_3. In fact, such behaviors have also been observed in the case of superconducting metal hydrides, where a key characteristic is that a high T_c is always accompanied by high contribution of hydrogen to the total DOS, such as in LaH_{10}, YH_{10} [4–7,49–53].

IV. CONCLUSIONS

In summary, the phase diagram of Y-S systems from atmospheric pressure to 50 GPa is extensively explored by using a combination study of crystal structure predictions and first-principle calculations. The structure searches at ambient pressure have predicted five new stable compounds with stoichiometries Y_7S_6, Y_6S_5, Y_7S_8, Y_6S_7, and Y_5S_6. Additionally, two pressure-stabilized compounds, Y_3S_2 and YS_3, are predicted to possess exotic properties. Y_3S_2 becomes energetically stable at 6 GPa, which is found to be a layer-structured magnetic electride. The layered Y_3S_2 transforms into a three-dimensional structure at 17 GPa accompanied by the disappearance of magnetism and localized interstitial electrons. Interestingly, YS_3 is predicted to be a potential superconductor with T_c of 18.5 K at 50 GPa, close to the maximum value (17 K) observed in elemental Y at 89.3 GPa and S at 160 GPa. It is notable that the pressure needed to realize the superconductivity in YS_3 is much lower than those in corresponding elements, which means that it is much easier to achieve in experiments. Analysis shows that the coupling of electrons of S atoms and the vibrations of Y atoms mainly contribute to the superconductivity of YS_3. The current results

are expected to guide the future experimental study on Y-S compounds under pressure.

ACKNOWLEDGMENTS

The authors acknowledge funding from the National Natural Science Foundation of China under Grants No. 12074154, No. 11722433, No. 11804128, and No. 11804129; the Six Talent Peaks Project and 333 High-Level Talents Project of Jiangsu Province; and the Science and Technology Project of Xuzhou under Grant No. KC19010. All the calculations were performed at the High Performance Computing Center of the School of Physics and Electronic Engineering of Jiangsu Normal University.

[1] A. Drozdov, M. Eremets, I. Troyan, V. Ksenofontov, and S. I. Shylin, Nature (London) **525**, 73 (2015).
[2] I. Errea, M. Calandra, C. J. Pickard, J. Nelson, R. J. Needs, Y. Li, H. Liu, Y. Zhang, Y. Ma, and F. Mauri, Phys. Rev. Lett. **114**, 157004 (2015).
[3] T. Jarlborg and A. Bianconi, Sci. Rep. **6**, 24816 (2016).
[4] H. Liu, I. I. Naumov, R. Hoffmann, N. Ashcroft, and R. J. Hemley, Proc. Natl. Acad. Sci. USA **114**, 6990 (2017).
[5] Z. M. Geballe, H. Liu, A. K. Mishra, M. Ahart, M. Somayazulu, Y. Meng, M. Baldini, and R. J. Hemley, Angew. Chem. **130**, 696 (2018).
[6] H. Liu, I. I. Naumov, Z. M. Geballe, M. Somayazulu, J. S. Tse, and R. J. Hemley, Phys. Rev. B **98**, 100102(R) (2018).
[7] I. Errea, F. Belli, L. Monacelli, A. Sanna, T. Koretsune, T. Tadano, R. Bianco, M. Calandra, R. Arita, F. Mauri *et al.*, Nature (London) **578**, 66 (2020).
[8] H. Wang, S. T. John, K. Tanaka, T. Iitaka, and Y. Ma, Proc. Natl. Acad. Sci. USA **109**, 6463 (2012).
[9] Y. Li, J. Hao, H. Liu, S. T. John, Y. Wang, and Y. Ma, Sci. Rep. **5**, 9948 (2015).
[10] D. Y. Kim, R. H. Scheicher, and R. Ahuja, Phys. Rev. Lett. **103**, 077002 (2009).
[11] C. Heil, S. di Cataldo, G. B. Bachelet, and L. Boeri, Phys. Rev. B **99**, 220502(R) (2019).
[12] H. Fujihisa, H. Yamawaki, M. Sakashita, A. Nakayama, T. Yamada, and K. Aoki, Phys. Rev. B **69**, 214102 (2004).
[13] O. Zakharov and M. L. Cohen, Phys. Rev. B **52**, 12572 (1995).
[14] V. V. Struzhkin, R. J. Hemley, H.-k. Mao, and Y. A. Timofeev, Nature (London) **390**, 382 (1997).
[15] J. Michiels and K. Gschneidner, Jr., J. Alloys Compd. **247**, 9 (1997).
[16] N. L. Eatough, A. W. Webb, and H. T. Hall, Inorg. Chem. **8**, 2069 (1969).
[17] K. Range and R. Leeb, Z. Naturforsch., B **30**, 889 (1975).
[18] B. Sahoo, K. Joshi, and S. C. Gupta, J. Appl. Phys. **115**, 123502 (2014).
[19] P. Roedhammer, W. Reichardt, and F. Holtzberg, Phys. Rev. Lett. **40**, 465 (1978).
[20] F. Hulliger and G. Hull Jr., Solid State Commun. **8**, 1379 (1970).
[21] Y. Qi, Z. Xiao, J. Guo, H. Lei, T. Kamiya, and H. Hosono, EPL **121**, 57001 (2018).
[22] W. Zhang, A. R. Oganov, A. F. Goncharov, Q. Zhu, S. E. Boulfelfel, A. O. Lyakhov, E. Stavrou, M. Somayazulu, V. B. Prakapenka, and Z. Konôpková, Science **342**, 1502 (2013).
[23] J. Lin, Z. Zhao, C. Liu, J. Zhang, X. Du, G. Yang, and Y. Ma, J. Am. Chem. Soc. **141**, 5409 (2019).
[24] M.-S. Miao, Nat. Chem. **5**, 846 (2013).
[25] L. Zhang, Y. Wang, J. Lv, and Y. Ma, Nat. Rev. Mater. **2**, 17005 (2017).
[26] C. Liu, X. Song, Q. Li, Y. Ma, and C. Chen, Phys. Rev. Lett. **124**, 147001 (2020).
[27] Y. Wang, J. Lv, L. Zhu, and Y. Ma, Phys. Rev. B **82**, 094116 (2010).
[28] Y. Wang, J. Lv, L. Zhu, and Y. Ma, Comput. Phys. Commun. **183**, 2063 (2012).
[29] B. Gao, P. Gao, S. Lu, J. Lv, Y. Wang, and Y. Ma, Sci. Bull. **64**, 301 (2019).
[30] J. Shi, W. Cui, S. Botti, and M. A. L. Marques, Phys. Rev. Mater. **2**, 023604 (2018).
[31] J. Shi, W. Cui, J. Hao, M. Xu, X. Wang, and Y. Li, Nat. Commun. **11**, 3164 (2020).
[32] W. Cui, T. Bi, J. Shi, Y. Li, H. Liu, E. Zurek, and R. J. Hemley, Phys. Rev. B **101**, 134504 (2020).
[33] B. Liu, W. Cui, J. Shi, L. Zhu, J. Chen, S. Lin, R. Su, J. Ma, K. Yang, M. Xu, J. Hao, A. P. Durajski, J. Qi, Y. Li, and Y. Li, Phys. Rev. B **98**, 174101 (2018).
[34] W. Cui and Y. Li, Chin. Phys. B **28**, 107104 (2019).
[35] J. P. Perdew, K. Burke, and M. Ernzerhof, Phys. Rev. Lett. **80**, 891 (1998).
[36] P. E. Blöchl, Phys. Rev. B **50**, 17953 (1994).
[37] G. Kresse and J. Furthmüller, Comput. Mater. Sci. **6**, 15 (1996).
[38] H. J. Monkhorst and J. D. Pack, Phys. Rev. B **13**, 5188 (1976).
[39] P. Giannozzi, S. Baroni, N. Bonini, M. Calandra, R. Car, C. Cavazzoni, D. Ceresoli, G. L. Chiarotti, M. Cococcioni, I. Dabo *et al.*, J. Phys.: Condens. Matter **21**, 395502 (2009).
[40] R. Dynes, Solid State Commun. **10**, 615 (1972).
[41] K. Momma and F. Izumi, J. Appl. Crystallogr. **44**, 1272 (2011).
[42] Y. Chen, Q.-M. Hu, and R. Yang, Phys. Rev. Lett. **109**, 157004 (2012).
[43] A. Jayaraman and R. Sherwood, Phys. Rev. **134**, A691 (1964).
[44] B. Johansson and A. Rosengren, Phys. Rev. B **11**, 2836 (1975).
[45] Y. Ge, S. Guan, and Y. Liu, New J. Phys. **19**, 123020 (2017).
[46] See Supplemental Material at http://link.aps.org/supplemental/10.1103/PhysRevResearch.2.043435 for the structures, electronic properties, and phonon dispersions of five stable compounds at ambient pressure; the charge transfers and the structure information of seven stable compounds; and other details.
[47] S. Rettig and J. Trotter, Acta Crystallogr., Sec. C **43**, 2260 (1987).
[48] N. W. Ashcroft, Phys. Rev. Lett. **92**, 187002 (2004).
[49] A. Drozdov, P. Kong, V. Minkov, S. Besedin, M. Kuzovnikov, S. Mozaffari, L. Balicas, F. Balakirev, D. Graf, V. Prakapenka *et al.*, Nature (London) **569**, 528 (2019).

[50] M. Somayazulu, M. Ahart, A. K. Mishra, Z. M. Geballe, M. Baldini, Y. Meng, V. V. Struzhkin, and R. J. Hemley, Phys. Rev. Lett. **122**, 027001 (2019).

[51] F. Peng, Y. Sun, C. J. Pickard, R. J. Needs, Q. Wu, and Y. Ma, Phys. Rev. Lett. **119**, 107001 (2017).

[52] H. Song, D. Duan, T. Cui, and V. Z. Kresin, Phys. Rev. B **102**, 014510 (2020).

[53] A. M. Shipley, M. J. Hutcheon, M. S. Johnson, R. J. Needs, and C. J. Pickard, Phys. Rev. B **101**, 224511 (2020).